




Cite this: *Nanoscale*, 2023, **15**, 1890

## A synergistic therapeutic nano-eyedrop for dry eye disease based on ascorbic acid-coupled exosomes†

Fang Ma,<sup>‡a,b</sup> Jing Feng,<sup>‡a,b</sup> Xi Liu,<sup>c</sup> Ying Tian,<sup>a,b</sup> Wen-Jing Wang,<sup>d,b</sup> Fu-Xiao Luan,<sup>a,b</sup> Ying-Jie Wang,<sup>a,b</sup> Wei-Qiang Yang,<sup>a,b</sup> Jing-Yi Bai,<sup>a,e</sup> Yi-Quan Zhang<sup>a,b</sup> and Yong Tao \*<sup>a</sup>

Dry eye disease (DED), a complex ocular surface disease with a high prevalence rate, is associated with corneal injury, excess oxidative stress and inflammation. Current therapeutic strategies, including artificial tears and anti-inflammatory agents, are unable to address all the deleterious factors or to achieve a clinical cure due to their temporary or side effects. Here, we prepared a multiple-functional eyedrop based on the deposition of gold nanoparticles (AuNPs) reduced by ascorbic acid (AA) onto the exosomal phospholipid membrane of mesenchymal stem cell (mExo)-derived exosomes *in situ* (mExo@AA). The therapeutic value of mExo@AA for DED was demonstrated in a mouse DED model. Combining the benefits of mExo and AA, mExo@AA effectively improves corneal epithelium recovery and anti-inflammation capacity, decreases corneal reactive oxygen species, and restores tear secretion without adverse effects. Thus, this study suggests that mExo@AA is effective and safe as a therapeutic agent for the treatment of DED.

Received 20th September 2022

Accepted 16th December 2022

DOI: 10.1039/d2nr05178h

[rsc.li/nanoscale](http://rsc.li/nanoscale)

### 1. Introduction

Dry eye disease (DED) is a multifactorial disease of tears and the ocular surface that results in symptoms of discomfort, visual disturbance, and tear film instability with potential damage to the ocular surface.<sup>1</sup> Large-scale epidemiological studies have shown that DED affects 5% to more than 50% of the general population.<sup>2</sup> In China, up to 31% of the population aged 5 to 89 suffers from DED symptoms (approximately 371 million people).<sup>3</sup> In addition to diabetes and hypertension, DED is a chronic disease, with the potential risks of ocular infection and surface damage, such as corneal abrasion or ulceration in severe cases. This can lead to a reduction in the vision-related quality of life and interfere with daily activi-

ties.<sup>4</sup> Current treatments, including artificial tears for mild DED or the combination of glucocorticoids and immunosuppressants for moderate to severe DED, can temporarily relieve ocular surface symptoms and control ocular surface inflammation. However, these strategies cannot bring about a radical cure and/or cause side effects.<sup>5</sup> Therefore, there is an urgent need to develop a novel strategy for the treatment of DED.

The mechanism of DED is associated with several processes, such as ocular surface damage and inflammation. Recently, mesenchymal stem cell-derived exosomes (mExo) have received growing attention due to their repair promoting and anti-inflammatory effects.<sup>6–8</sup> Certain proteins and microRNAs carried by mExo have so far been proposed as key mediators of these effects, such as transmembrane enzymes CD73,<sup>9</sup> Wnt 4,<sup>10</sup> miR-204,<sup>11</sup> and miR-182.<sup>12</sup> Additionally, mExo have been applied in the field of ophthalmology to promote corneal wound healing,<sup>13</sup> inhibit neovascularization, and regulate autoimmune uveitis.<sup>14</sup> In particular, mExo have shown considerable promise as a treatment for DED, and several mechanisms of their therapeutic action have been studied. For example, Gong C. *et al.* demonstrated that exosomes derived from mouse adipose-derived mesenchymal stem cells alleviate a benzalkonium chloride-induced mouse dry eye model *via* inhibiting NLRP3 inflammasomes.<sup>15</sup> Liu and collaborators reported that mExo provided substantial relief on refractory plant-versus-host disease-associated DED through the activation of the IL-6/IL-6R/Stat3 pathway and also induced differentiation of inflammatory M1 macrophages to immunosuppressive M2 macrophages.<sup>11</sup>

<sup>a</sup>Department of Ophthalmology, Beijing Chaoyang Hospital, Capital Medical University, Beijing 100020, P. R. China. E-mail: taoyong@bjcyh.com

<sup>b</sup>Key Laboratory of Biochemical Engineering, Institute of Process Engineering, Chinese Academy of Sciences, Beijing 100080, P. R. China

<sup>c</sup>Research Center for Tissue Repair and Regeneration affiliated to the Medical Innovation Research Department and 4th Medical Center, PLA General Hospital and PLA Medical College, Beijing 100048, P. R. China

<sup>d</sup>Department of Neurosurgery, Health Science Center, The First Affiliated Hospital of Shenzhen University, Shenzhen Second People's Hospital, Shenzhen 518035, P. R. China

<sup>e</sup>Department of Ophthalmology, Beijing Huairou Hospital, Capital Medical University, Beijing 101400, P. R. China

†Electronic supplementary information (ESI) available. See DOI: <https://doi.org/10.1039/d2nr05178h>

\*These authors contributed equally to this work.



However, owing to the complexity of the etiology of DED, its treatment within a short period of time based on the pro-repair and anti-inflammatory functions of mExo is still challenging. Excessive production of reactive oxygen species (ROS) also constitutes an important contributor to DED.<sup>16,17</sup> Several ROS scavengers, like cerium oxide and mitochondrial quinones, have been employed to scavenge ROS for the treatment of DED.<sup>18,19</sup> As an excellent antioxidant ingredient in human tears, ascorbic acid (AA) can effectively maintain the free radical balance in the human body by scavenging ROS or generating stable compounds when reacting with ROS, and show substantial biosafety.<sup>20</sup> AA has protective benefits in the treatment of corneal diseases, such as UV irradiation,<sup>21</sup> chemical corneal burns,<sup>22</sup> corneal neovascularization,<sup>23</sup> and inflammation,<sup>24</sup> as well as enhancing repair of the corneal epithelium in clinical practice.<sup>25</sup> Therefore, the combination of mExo and AA offers the possibility to effectively overcome the limitations associated with monotherapies and employ multiple therapeutic strategies.

In this study, we report on the creation and use of an advanced eyedrop composed of AA-coupled mExo (mExo@AA) towards the treatment of DED. mExo@AA was prepared based on the deposition of gold nanoparticles (AuNPs) reduced by AA onto the exosomal phospholipid membrane *in situ*. *In vitro* and *in vivo* results demonstrated that mExo@AA alleviated DED through multi-faceted effects, including repairing ocular surface damage, scavenging ROS, and reducing inflammation. Moreover, assessments of its cell toxicity and tissue biocompatibility after topical application confirmed its safety. This study provides new information to develop next-generation therapeutic agents towards DED.

## 2. Results and discussion

### 2.1. Association between inflammation and excessive ROS in patients with dry eye disease

Several recent studies have reported the upregulation of inflammatory cytokines and excessive ROS in DED animal models,<sup>16,17</sup> providing direct evidence to support the comorbidity of ROS and inflammation. We collected these samples from patients with DED ( $n = 12$ ) and from control subjects ( $n = 12$ ) and quantified the inflammatory cytokines and ROS level (Fig. 1a). As shown in Fig. 1b, in patients with DED, the levels of IL-6, IL-1 $\beta$  and ROS expression were up-regulated 3.5, 2.8 and 1.3 times higher than those of healthy controls, respectively. These results show that inflammation and ROS in dry eye patients have a higher overexpression than those in healthy individuals. Current treatments can only temporarily relieve ocular surface symptoms and control ocular surface inflammation in a single aspect of the disease, failing to produce a radical cure. Therefore, it is necessary to construct a new strategy that synergistically achieves ocular surface repair, anti-inflammation, and ROS clearance.

### 2.2. Preparation and characterization of mExo and mExo@AA

mExo can be loaded with AA, a small water-soluble molecule, using several processes, including sonication, co-incubation,

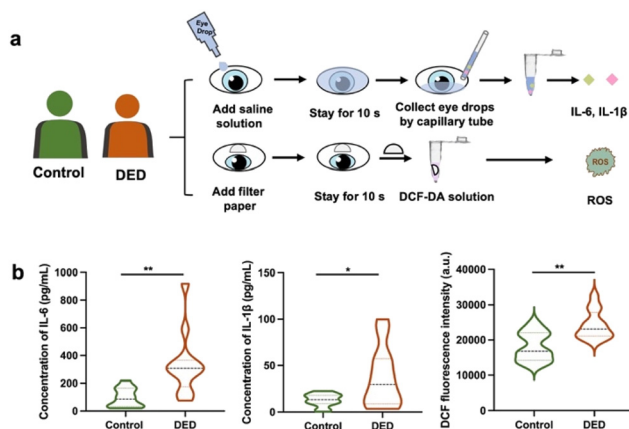


**Fig. 1** (a) Schematic for the collection of human tears and conjunctival cells, and subsequent assays for inflammatory cytokines and ROS in the control and DED groups. (b) ELISA measurement of pro-inflammatory cytokines IL-6 and IL-1 $\beta$  in human tears and ROS in conjunctival cells. \*\* $p < 0.01$ , \* $p < 0.05$ , n.s. means not significant, and analyzed using one-way ANOVA.

and electroporation. However, the procedures are complex and show a low loading efficiency and damage to the morphology of mExo. A novel and convenient surface-modification strategy is needed to overcome these issues. In the production of AuNPs, AA is a better stabilizer than NaBH<sub>4</sub> due to its mild reducing property and greater ligand characteristics. Previous studies have shown that AA acts as a reducing and protective reagent in the synthesis of AuNPs.<sup>26</sup>

In this study (Fig. 2a), Au<sup>3+</sup> was used to deposit AA on the surface of mExo using DSPE-PEG-SH as a handle, with AA used as a reducing agent and a protective agent to reduce the AuNPs. AA loaded on the mExo formed mExo@AA in order to ameliorate DED through multiple effects, including repairing ocular surface damage, scavenging ROS, and reducing inflammation (Fig. 2b).

The mExo isolated in this study exhibited a typical saucer-shaped morphology, with an average diameter of approximately 150 nm (Fig. 2c, left). After the reaction (1 : 1 ratio of NaBH<sub>4</sub> : AA), 10 nm AA-protective AuNPs were formed and deposited uniformly over the mExo surface without changing their morphology (Fig. 2c, right). Fig. 2d shows the size and zeta potential of mExo and mExo@AA. Compared with unmodified exosomes, the hydrodynamic diameter of mExo@AA was almost unchanged, indicating that the grafting of AA did not influence the size and distribution of the mExo (Fig S1†). Moreover, the mean size of mExo@AA was 100–150 nm, which is favorable for the accumulation of mExo@AA in cells. After AA loading, the zeta potential was slightly higher, further confirming that the mExo were modified with AA-protective AuNPs. Both the mExo and mExo@AA were positive for exosomal marker proteins ALIX,  $\beta$ -actin, and TSG 101, while they were negative for GM130, a protein found in the Golgi apparatus and present in cell lysates<sup>27</sup> (Fig. 2e), confirming that AA loading did not influence the molecular features of mExo and no contaminating cellular debris was present in the prepa-



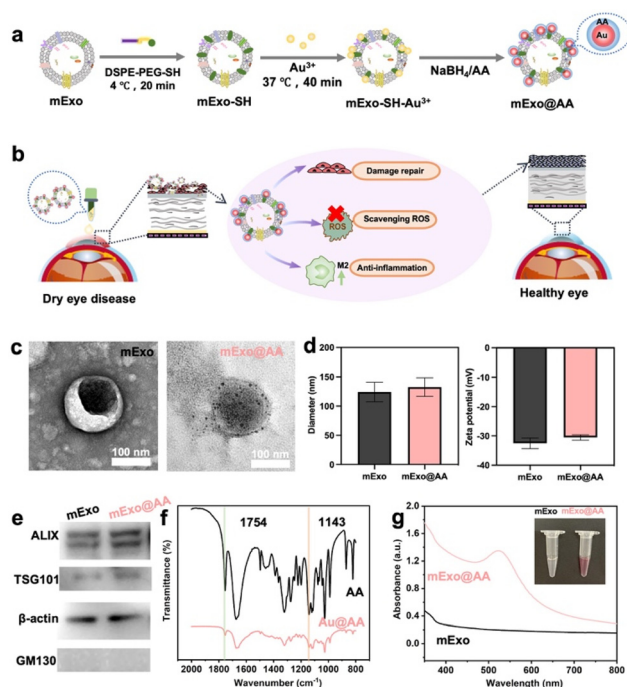


**Fig. 2** (a) Schematic showing the steps in the synthesis of mExo@AA. (b) mExo@AA eyedrops alleviate DED by (1) repairing ocular surface damage, (2) scavenging ROS, and (3) reducing inflammation. (c) TEM images of mExo (left) and mExo@AA (right) stained with uranyl acetate. (d) Particle size (left) and zeta potential (right) of mExo and mExo@AA. (e) Western blot images of mExo and mExo@AA; ALIX,  $\beta$ -actin and TSG 101 are markers for exosomes, while GM130 is negative. (f) FTIR spectra of AA and Au@AA;  $1754\text{ cm}^{-1}$  is the characteristic peak of C=O and  $1143\text{ cm}^{-1}$  is the characteristic peak of OH. (g) UV-Vis absorption spectra and images (top right) of mExo and mExo@AA.

ration of mExo and mExo@AA. Finally, mExo@AA showed reasonable stability without detectable changes in the particle size or zeta potential after storage in PBS at  $-80\text{ }^{\circ}\text{C}$  (Fig. S2†).

To demonstrate more simply and clearly that Au can be used as a connecting agent for AA and mExo, we first showed that AA could be used as a reducing and protective agent for Au using FTIR spectroscopy, and then that Au could be loaded on mExo using UV-Vis spectroscopy. The absorption bands at  $1754\text{ cm}^{-1}$  and  $1143\text{ cm}^{-1}$  in the FTIR spectra of both AA and Au@AA are attributable to C=O and OH vibrations, respectively, which are characteristic of AA, indicating that AA was successfully loaded on the AuNPs as a protective agent (Fig. 2f).<sup>28</sup> Meanwhile, the ratio of C=O/OH increased from 0.75 to 1.03, indicating that some AA had been oxidized, detailed data are shown in Table 1. Overall, the FTIR spectrum illustrated that AA acted as both a reducing and a protective agent. As shown in Fig. 2g, the UV-Vis spectrum of mExo@AA has a characteristic absorption peak corresponding to AuNPs at 520 nm, indicating that the AuNPs were successfully incorporated onto the mExo. Therefore, these results indicate that AA was successfully loaded on the surface of mExo based on the AuNPs functioning as a handle.

**Table 1** Calculated and experimental vibrational band positions of AA

	C=O	OH	Ratio of C=O/OH
Band position ( $\text{cm}^{-1}$ )	1754	1143	—
Integral region ( $\text{cm}^{-1}$ )	1735–1768	1128–1175	—
AA	3118	4179	0.75
Au@AA	1778	1732	1.03

### 2.3. AA loading and ROS scavenging capacities of mExo@AA

We investigated the influence of the  $\text{NaBH}_4$ :AA ratio on the loading capacity of AA. As shown in Fig. 3a, with an increase in the AA content, the color of mExo@AA changed from orange to red and finally to blue, which was related to the size of the AuNPs. When the AA content was low, the reducing agent was mainly  $\text{NaBH}_4$ , which exhibited a strong reduction ability, resulting in smaller AuNPs. With more AA content, the reducing strength of  $\text{NaBH}_4$  was decreased, resulting in the formation of larger AuNPs. The loading efficacy of AA increased gradually to about  $509\text{ nM mg}^{-1}$  with a 1 : 1 ratio of  $\text{NaBH}_4$  to AA, but decreased as the ratio continued to increase (Fig. 3b). Because an excessive AA content resulted in poor reduction ability, the generation of larger AuNPs with smaller specific surfaces led to a lower AA loading capacity, and the particle size of AuNPs in  $\text{N}_{10}:\text{A}_0$  was  $\sim 5\text{ nm}$  and that in  $\text{N}_0:\text{A}_{10}$  was  $\sim 30\text{ nm}$  (Fig. S3†), which supports this explanation. Therefore, in the following experiments, we chose  $\text{NaBH}_4$ :AA at a ratio of 1 : 1 as the reducing agent.

In general, the ROS scavenging ability of mExo@AA was closely related to the loading efficacy of AA. Fig. 3c shows that the ROS scavenging efficiency of mExo@AA first increased and then decreased at a given concentration of mExo@AA ( $10\text{ }\mu\text{g mL}^{-1}$ ), which was consistent with the AA content of mExo@AA. The ROS scavenging capacity of mExo@AA was also affected by its concentration, increasing from 40% to about 80% as the concentration increased from 0.01 to  $0.5\text{ mg mL}^{-1}$ ,

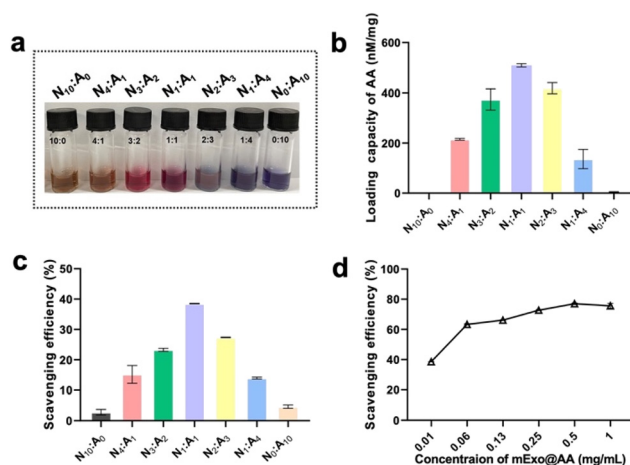


**Fig. 3** (a) Images, (b) AA loading capacity, and (c) ROS scavenging efficiency at different ratios of  $\text{NaBH}_4$ :AA (10 : 0, 4 : 1, 3 : 2, 1 : 1, 2 : 3, 1 : 4, and 0 : 10, respectively). (d) ROS scavenging efficiency at different mExo@AA concentrations.



with a maximum scavenging capacity evident at 0.5 mg mL<sup>-1</sup> (Fig. 3d). The complex could not achieve a high ROS scavenging efficiency of AA, but its efficiency was greatly improved compared with mExo (Fig. S4†).

#### 2.4. Effect of mExo@AA on corneal repair and ROS scavenging *in vitro*

Prior to investigating the corneal repair effect and ROS removal capacity of mExo@AA, we assessed the uptake of mExo@AA by HCECs. As shown in Fig. 4a, DiD-labelled mExo@AA with red fluorescence was mostly localized around the perinuclear region (blue fluorescence) after incubation with HCECs for 12 h. To explore the corneal repair effect of mExo@AA *in vitro*, the scratch assay on a monolayer of HCECs was performed using equivalent amounts of mExo, AA, and saline as controls. We observed that re-epithelialization in monolayers treated with mExo@AA was significantly accelerated, with 70.90 ± 4.18% of the wound area closed, compared with the outcomes corresponding to saline (11.67 ± 7.35%),

mExo (55.63 ± 7.52%), and AA (31.23 ± 6.46%) treatments (Fig. 4b and d). These results indicated the excellent re-epithelialization properties of mExo@AA, attributed to the well-known migration promoting properties of mExo and AA, especially mExo.<sup>29,30</sup>

Apart from the need for corneal repair, ROS scavenging is also a necessity due to the susceptibility to oxidative stress of the anterior segment of the eye, which produces excess unstable ROS that leads to cellular damage in DED.<sup>31</sup> In this study, we explored the intracellular ROS scavenging efficacy of mExo@AA in H<sub>2</sub>O<sub>2</sub>-treated HCECs. As shown in Fig. 4c, the saline and mExo groups showed obvious green fluorescence (labelled with the DCF probe), indicating a higher ROS content in HCECs. In contrast, the green fluorescence intensity was minimal following the treatment with AA or mExo@AA, indicating their excellent intracellular ROS scavenging efficacy. The corresponding statistical analysis is presented in Fig. 4e, which quantitatively shows a similar tendency as indicated by the CLSM images. Furthermore, mExo@AA showed excellent biocompatibility even at a high concentration of 1000 µg mL<sup>-1</sup> on HCECs, as demonstrated by the CCK-8 assay (Fig. 4f). The above results indicated that mExo@AA had abilities of pro-wound healing, ROS scavenging and biocompatibility.

#### 2.5. Anti-inflammatory effect of mExo@AA *in vitro*

Macrophage-mediated inflammatory response, which can result in epithelial cell injuries and/or degeneration, is found to play a crucial role in DED.<sup>32</sup> Previous studies have shown that mExo can modulate the macrophage immunophenotype by promoting the differentiation of macrophages into particular phenotypes,<sup>11,33</sup> and the effects of AA on the immune response in ocular diseases have also been investigated in a few studies.<sup>34,35</sup> In the current study, LPS-induced mouse peritoneal macrophages were cultured under the different treatments to evaluate the effects of mExo@AA on macrophages. Specifically, the drugs used in the treatments were added to the macrophages at 12 h after LPS stimulation, instead of the beginning of the culturing process. As shown in Fig. 5, macrophages cultured with mExo showed increased expression of CD 206, which is associated with M2 inflammation-resolving macrophage immunophenotypes. Furthermore, AA increased the percentage of M2 cells, which can reduce inflammation by removing the ROS involved in the deterioration of ocular surface cells,<sup>36</sup> and flow cytometry results indicated that the mExo@AA treatment resulted in a greater increase in the percentage of M2 cells (56.72%) than mExo (45.58%,  $p = 0.005$ ) and AA (34.93%,  $p < 0.0001$ ) treatments due to the synergistic effects of mExo and AA (Fig. 5). We also investigated the effect of mExo@AA treatment on the expression of inflammation mediators linked to the inflammation of DED. As shown in Fig. 5c, mExo, AA, and mExo@AA all significantly reduced the pro-inflammatory cytokines IL-6 and IL-1β in the supernatant. Notably, although mExo@AA was the most efficient in reducing the inflammatory factors, it did not vary significantly with the mExo group, which may be related to the low overall concentrations of the inflammatory factors in the supernatant.

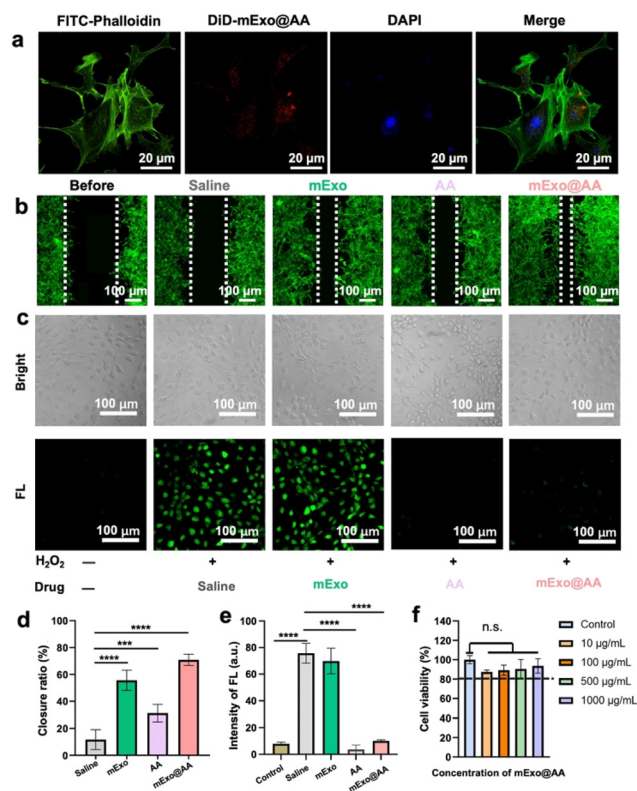


**Fig. 4** (a) CLSM images of intracellular internalization of mExo@AA in HCECs (green: FITC-labelled cell membrane, red: DiD-labelled mExo@AA, blue: DAPI-labelled cell nucleus). (b) Scratch assay and (d) quantitative closure ratio of HCECs treated with saline, mExo, AA and mExo@AA. (c) Representative CLSM images and (e) quantitative analysis of ROS scavenging in HCECs treated with saline, mExo, AA and mExo@AA. The upper and lower panels show bright field and CLSM images, respectively. Error bars represent the standard deviation ( $n = 3$ ). (f) Viability of HCECs treated with different concentrations of mExo@AA. \*\*\*\* $p < 0.0001$ , \*\*\* $p < 0.001$ , n.s. means not significant, and analyzed using one-way ANOVA.



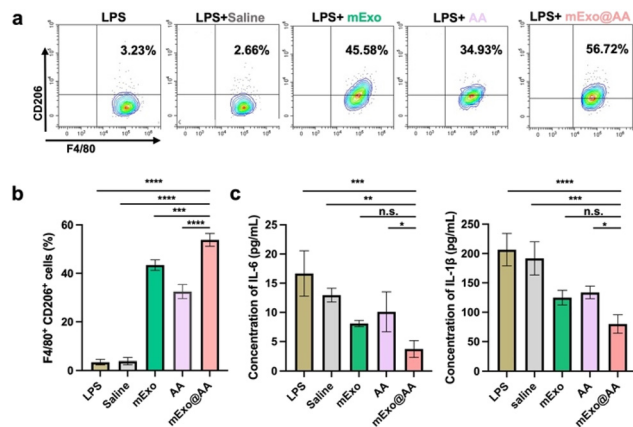


**Fig. 5** (a) and (b) Flow cytometry showing CD 206 expression in LPS-induced macrophages treated with saline, mExo (1 mg mL<sup>-1</sup>), AA (509 nM mL<sup>-1</sup>), and mExo@AA (1 mg mL<sup>-1</sup>). The error bar represents standard deviations ( $n = 3$ ). (c) ELISA measurement of the inflammatory cytokines IL-6 and IL-1 $\beta$  in the supernatant. \*\*\*\* $p < 0.0001$ , \*\*\* $p < 0.001$ , \*\* $p < 0.01$ , \* $p < 0.05$ , n.s. means not significant, analyzed using one-way ANOVA.

These observations indicate that mExo@AA can enhance the polarization of M2 macrophages, and thus reduce inflammation.

## 2.6. mExo@AA suppresses DED in BAC-induced mice

To examine whether mExo@AA can be used as an effective therapy for DED, the BAC-induced dry eye mouse model was chosen, because it had the essential clinical features of DED and is also stable and suitable for the evaluation of the treatment response.<sup>37</sup> Fig. 6a shows the process for establishing the BAC-induced DED model and subsequent treatments using different drugs. At 7 days after treatment, the evaluation of eye surface damage *via* fluorescein staining was performed under a slit lamp. The corneal surface would appear green under cobalt blue light if there was a wound. As shown in Fig. 6b and e, the cornea of mice in the control group (healthy eyes) exhibited a clear and deep profile, with almost no green dots visible. After inducing DED using BAC and treatment with saline, the cornea showed a diffused green dot staining profile in four areas, indicating severe corneal injury. The mExo@AA-treated DED mice exhibited less fluorescein staining compared with the BAC mice in the mExo and AA treatment groups ( $p < 0.01$  and  $p < 0.0001$ , respectively).

The overproduction of ROS results in ocular surface inflammation and tear film hyperosmolarity, eventually causing DED.<sup>31</sup> Therefore, scavenging excessive ROS is necessary to repair DED. The ROS scavenging efficacy of mExo@AA *in vivo* was measured using a DHE probe *via* fluorescence microscopy. As shown in Fig. 6c, compared with the saline-treated group, both the control (healthy eyes) and mExo@AA-treated groups showed negligible fluorescence, indicating the high ROS scavenging efficacy of mExo@AA. Notably, unlike *in vitro* ROS scavenging experiments, the AA and mExo groups still showed a high ROS fluorescence signal, indicating that DED could not be completely reversed after monotherapy with AA or mExo for 7

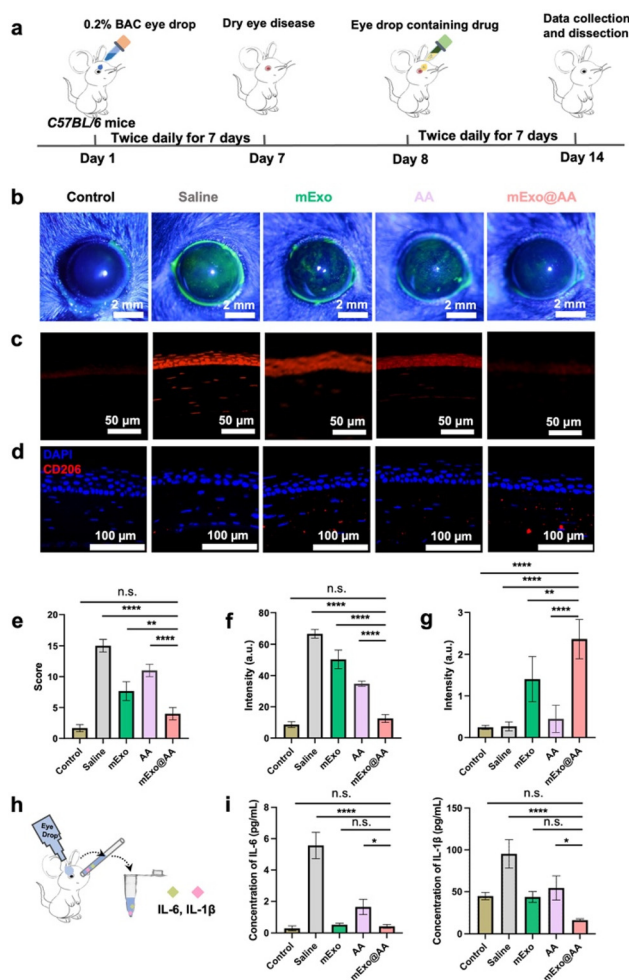


**Fig. 6** (a) Establishment schematic of BAC-induced DED mice. (b) Representative images of the corneal wound area stained with sodium fluorescein and (e) mean staining score of the eye surface in each group after treatment with saline, mExo (1 mg mL<sup>-1</sup>), AA (509 nM mL<sup>-1</sup>), and mExo@AA (1 mg mL<sup>-1</sup>). (c) Fluorescence images (DHE was used as the probe of ROS) and (f) quantitative statistics of the fluorescence intensity showing ROS scavenging efficiency. (d) Representative immunofluorescence staining images and (g) quantitative analysis of CD 206 fluorescence after the treatments (saline, mExo (1 mg mL<sup>-1</sup>), AA (509 nM mL<sup>-1</sup>), and mExo@AA (1 mg mL<sup>-1</sup>)) of injured murine cornea. Error bars represent the standard deviation ( $n = 6$ ). (h) Schematic for the collection of mouse tears. (i) ELISA measurement of inflammatory cytokines IL-6 and IL-1 $\beta$  in murine tears. \*\*\*\* $p < 0.0001$ , \*\*\* $p < 0.001$ , \*\* $p < 0.01$ , \* $p < 0.05$ , n.s. means not significant, analyzed using one-way ANOVA.

days. These observations demonstrated that only the combined treatment of mExo and AA could completely scavenge ROS levels *in vivo*. Corresponding statistical analyses performed using GraphPad Prism 5.0 software showed the same tendency as the CLSM images (Fig. 6f).

We next investigated the effects of saline, mExo, AA, and mExo@AA on the macrophage immunophenotype in the BAC-induced DED model. Consistent with the LPS-induced macrophage immunophenotype observed *in vitro*, histologic studies demonstrated significantly greater CD206 counts (a marker of



M2 cells) in the corneas of mExo@AA-treated mice than in those treated with mExo ( $p = 0.0059$ ) or AA ( $p < 0.0001$ ) alone (Fig. 6d and g); the negative expression of CD 206 in the control group implied low inflammation in healthy eyes. We collected the mouse tears and measured the inflammation mediators (Fig. 6h), finding that the pro-inflammatory cytokines IL-6 and IL-1 $\beta$  showed the same tendency as CD 206 (Fig. 6i). mExo@AA-induced M2 macrophage polarization may therefore have suppressed inflammatory responses and enhanced subsequent reparative activities, thus slowing DED progression. In summary, both the *in vitro* and *in vivo* experiments showed that mExo were superior in corneal pro-repair and anti-inflammation, while AA was better in scavenging ROS. The combination of mExo and AA (mExo@AA) showed superior efficacy to either component alone in alleviating DED in BAC-induced mice by accelerating corneal repair, scavenging ROS and promoting anti-inflammation ability.

The ocular surface of patients with DED suffers from extensive inflammatory destruction, resulting in defects in the epithelium, stromal swelling, and decreased tear volume. Histological analysis revealed that, in contrast to the treatment of DED mice with saline, mExo, or AA, the mExo@AA treatment minimized corneal damage, increased the thickness of the central cornea, and restored the stromal layer such that it became well-organized (Fig. 7a, b, and c). The level of tear secretion was measured using the cotton thread method. The administration of mExo@AA eyedrops significantly increased tear secretion, compared with mExo or AA alone, with a wet length of about 6 mm in 30 s, almost reaching the baseline observed in normal mouse eyes (Fig. 7d and e). These observations indicated the superior alleviating efficacy in the BAC-induced DED of mExo@AA. Finally, slices of the major organs of the mExo@AA-treated mice were subjected to hematoxylin

and eosin staining (Fig. S5 $\dagger$ ). The results revealed that these mice showed negligible pathological changes at 7 days after treatment, demonstrating the desirable biocompatibility of the mExo@AA composite.

### 3. Experimental

#### 3.1. Materials

Gold chloride trihydrate ( $\text{HAuCl}_4 \cdot 4\text{H}_2\text{O}$ ), AA and hydrogen peroxide solution (30 wt%) were purchased from Sinopharm Chemical Reagent Beijing Co., Ltd (China). Sodium borohydride was purchased from Tianjin Jinke Fine Chemical Research Institute (Tianjin, China). Thiol-terminated 1,2-distearoyl-*sn*-glycero-3-phosphoethanolamine-poly(ethylene glycol) (DSPE-PEG-SH,  $M_w$  2000) was obtained from Shanghai ZZBIO Co., Ltd (Shanghai, China). A BCA Protein Assay Kit was provided by Thermo Fisher Scientific. 1,1'-Diocetadecyl-3,3,3',3'-tetramethylindodicarbocyanine,4-chlorobenzenesulfonate salt (DiD) was purchased from Beijing FANBO biochemicals Co., Ltd. Dulbecco's modified Eagle's medium (DMEM) was purchased from HyClone. Fetal bovine serum was purchased from Gibco, and penicillin-streptomycin was purchased from Corning Life Sciences. Anti- $\beta$  actin rabbit monoclonal antibody, anti-TSG 101, anti-GM130 and anti-ALIX were purchased from BD Biosciences.

#### 3.2. Cell culture and mExo extraction

Mouse MSC cells were provided by Procell Life Science & Technology Co., Ltd and cultured in DMEM containing 10% exosome-free FBS, penicillin ( $100 \text{ U mL}^{-1}$ ) and streptomycin ( $100 \text{ mg mL}^{-1}$ ). The cells were incubated at  $37^\circ\text{C}$  in a cell incubator with 5%  $\text{CO}_2$  and expanded in three to five passages for usage. Exosomes were prepared and purified according to a previous study.<sup>38</sup> The culture supernatant was collected followed by a gradient centrifugation at  $4^\circ\text{C}$ , including  $300g$  for 10 min,  $2000g$  for 20 min,  $10\,000g$  for 30 min and  $100\,000g$  for 1 h. The pellet was washed twice with phosphate-buffered saline (PBS) and the prepared exosomes were stored at  $-80^\circ\text{C}$ .

#### 3.3. Fabrication of mExo@AA

DSPE-PEG-SH was dispersed in ethanol at a concentration of  $10 \text{ mg mL}^{-1}$ .  $10 \mu\text{L}$  of DSPE-PEG-SH solution was added to native mExo ( $1 \text{ mL}$ ,  $0.2 \text{ mg mL}^{-1}$ ) under gentle rotation at  $4^\circ\text{C}$  for 20 min. Then,  $\text{HAuCl}_4$  solution ( $50 \mu\text{L}$ , 1%) was added to the mixture and incubated at  $37^\circ\text{C}$  for 40 min. Subsequently, the residual DSPE-PEG-SH and  $\text{HAuCl}_4$  were removed by ultracentrifugation at  $100\,000g$  for 30 min and mExo-Au<sup>3+</sup> was resuspended in 2 mL of 0.01 M PBS solution.  $\text{NaBH}_4$  ( $53 \mu\text{M mL}^{-1}$ ) and AA ( $57 \mu\text{M mL}^{-1}$ ) solutions were prepared. After that,  $100 \mu\text{L}$  with different proportions of these two solutions (10:0, 2:1, 3:2, 1:1, 2:3, 1:4 and 0:10, v/v) were added to initiate a reduction reaction and gently stirred for 5 min. The residual  $\text{NaBH}_4$  and AA were removed by ultracentrifugation at  $100\,000g$  for 30 min and AA-loaded mExo (mExo@AA) was resuspended in 2 mL of 0.01 M PBS solution. Finally, mExo@AA was obtained and stored at  $-80^\circ\text{C}$ .

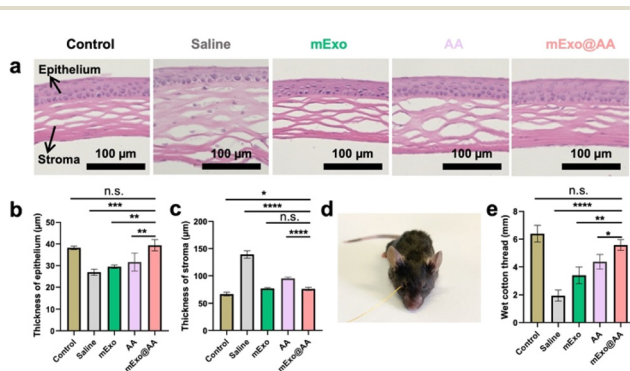


**Fig. 7** (a) Corneal sections based on H&E staining after the different treatments (saline, mExo ( $1 \text{ mg mL}^{-1}$ ), AA ( $509 \text{ nM mL}^{-1}$ ), and mExo@AA ( $1 \text{ mg mL}^{-1}$ )). Thicknesses of (b) epithelium and (c) stroma layers based on measurements performed using Graphpad. (d) Representative images corresponding to the cotton thread measurement of mice after treatment with saline, mExo, AA, and mExo@AA. (e) Cotton thread test showing a significant increase in the tear volume in BAC-induced mice treated with mExo@AA compared with the tear volumes corresponding to mice treated with saline, mExo, and AA. Error bars represent the standard deviation ( $n = 6$ ). \*\*\*\* $p < 0.0001$ , \*\*\* $p < 0.001$ , \*\* $p < 0.01$ , \* $p < 0.05$ , n.s. means no significance, analyzed by one-way ANOVA.



### 3.4. Characterization of mExo and mExo@AA

10  $\mu\text{L}$  of purified mExo and mExo@AA were dropped onto a carbon-coated copper grid and stained with 2% uranyl acetate for 2 min. The morphology was observed using a transmission electron microscope (TEM, HT7000, Hitachi, Japan) at 100 kV. NTA (Zetaview, Particle Metrix, Germany) was used to test their diameters and zeta potentials. The representative markers ( $\beta$ -actin, TSG 101, and ALIX) and the negative marker (GM130) of exosomes were analyzed by western blot. The absorbance and characteristic peaks were recorded using UV-Vis (Cary 5000, Varian) and FTIR (NICOLET iS 50, Thermo) spectrometers.

### 3.5. Loading capacity of AA

After the completion of the reduction reaction, the residual  $\text{NaBH}_4$  and AA were removed by centrifugation at 100 000g for 30 min. The concentrations of AA in the supernatant and solution before the reaction were measured using the Ascorbic Acid Assay Kit (Beijing Solarbio Science & Technology Co., Ltd). The loading capacity of AA was calculated using the following equation.

$$\text{Loading capacity} = (c_b - c_a)/c_{\text{mExo}} \text{ (nM mg}^{-1}\text{)}$$

where  $c_b$  and  $c_a$  are the concentrations of AA before and after the reaction and  $c_{\text{mExo}}$  is the concentration of mExo.  $\text{nM mg}^{-1}$  is the amount of AA on the surface of 1 mg of mExo.

### 3.6. Uptake of mExo@AA by human cultured corneal endothelial cells (HCECs)

The mExo@AA solution was stained with DiD for 1 h at 37  $^\circ\text{C}$ . The excess dye was removed using exosome spin columns (Thermo Fisher). HCECs were incubated with mExo@AA for 12 h, followed by fixation and imaging.

### 3.7. *In vitro* scratch wound assay

HCECs were seeded into 24-well plates with a density of  $5 \times 10^6$  per cell and cultured overnight. Then the cell monolayer was scratched using a sterile 10  $\mu\text{L}$  pipette tip and washed twice with PBS to remove the floating cells. After that, fresh medium containing different drugs, including saline, mExo ( $1 \text{ mg mL}^{-1}$ ), AA ( $509 \text{ nM mL}^{-1}$ , consistent with the concentration of AA in mExo@AA at  $1 \text{ mg mL}^{-1}$ ) and mExo@AA ( $1 \text{ mg mL}^{-1}$ ), but without a growth factor, was added and co-incubated for 12 h. The cytoskeleton was dyed with FITC-phalloidin and confocal laser scanning microscopy (CLSM) (Leica, Germany) was used to capture the scratch area picture. The wound area was measured using ImageJ software.

### 3.8. *In vitro* intracellular ROS scavenging

HCECs were seeded into 12-well plates with a density of  $10^4$  per well and cultured for 12 h at 37  $^\circ\text{C}$  with 5%  $\text{CO}_2$ . After that, the cells were treated with saline, mExo ( $1 \text{ mg mL}^{-1}$ ), AA ( $509 \text{ nM mL}^{-1}$ ) and mExo@AA ( $1 \text{ mg mL}^{-1}$ ) and incubation was continued for 12 h. After treating with  $\text{H}_2\text{O}_2$  ( $400 \mu\text{M}$ ) for 10 min, a 2'-7'-dichlorofluorescein diacetate (DCFH-DA) probe was added and incubated for 0.5 h at 37  $^\circ\text{C}$  in the dark. All the

concentration in the above description was the final concentration in the solution. For comparison, the group without any treatment was defined as the negative control group. Fluorescence microscopy images were observed using a CLSM (Leica, Germany). For quantitative results, the fluorescence intensity was measured using ImageJ software.

### 3.9. Cytotoxicity study

HCECs were plated in 96-well plates with a density of  $10^4$  and incubated for 12 h. Then the medium was placed with 100  $\mu\text{L}$  of DMEM containing different concentrations of mExo@AA (0, 10, 100, 500, and 1000  $\mu\text{g mL}^{-1}$ ). After culturing for 24 h, the cell viability was measured using a CCK-8 kit (Solarbio, China).

### 3.10. Mice and dry eye models

C57BL/6J male mice (6 to 8 weeks old) were purchased from Beijing Vital River Laboratory Animal Technology Co., Ltd and used for establishing dry eye models. Benzalkonium chloride (BAC) (Sigma-Aldrich, St Louis, MO, USA) was used as a drug to induce a dry eye model. Specifically, 5  $\mu\text{L}$  of 0.2% BAC solution was dropped into the mice's right eyes twice daily for 7 days. These mice were randomly assigned to different treatment groups with 5  $\mu\text{L}$  of eyedrop per eye, including saline, mExo ( $1 \text{ mg mL}^{-1}$ ), AA ( $509 \text{ nM mL}^{-1}$ ) and mExo@AA ( $1 \text{ mg mL}^{-1}$ ) and lasted for 7 days, twice a day. Besides, the healthy eye without any eyedrop treatment was used as the control group.

### 3.11. Murine ocular surface examination

Pentobarbital (0.05 mg per g body weight) was injected into the intraperitoneal region. After waiting for 5 min, the cotton thread test (Zone-Quick, Showa Yakuhin Kako, Tokyo, Japan) was performed to measure the tear quantity. The thread was held with a rectangular tweezer and put in the lateral canthus for 30 s. The cotton turned red after coming in contact with tears and the wetting length was measured in millimeters immediately. Wound closure was monitored after 7 days of treatment using fluorescein staining and photographed using a slit lamp microscope (Slit Lamp BX900; Haag-Streit, USA). The corneal epithelial damage area was divided into four parts, graded from 0 to 4 in each part.<sup>39</sup> Briefly, a grade of 0–4 was assigned to each quadrant: 0, absent; 1) slightly punctate staining <30 spots; 2) punctate staining >30 spots, but not diffuse; 3) severe diffuse staining but no positive plaque; and 4) positive fluorescein plaque-staining score. Six right eyes per group were examined and the average value was used for analysis. The total scores of four parts were summed as the final fluorescence score.

### 3.12. *In vivo* ROS scavenging

Dihydroethidium (DHE) was used as the probe to stain the ROS in the cornea. The fresh cornea was frozen with liquid nitrogen for 1 min and stored at  $-20 \text{ }^\circ\text{C}$ . Cryosections were washed with PBS three times and incubated with DCFH-DA at



37 °C for 30 min. Then the section was photographed using a CLSM (Leica, Germany).

### 3.13. Histological evaluation

After euthanasia, the eyes from different groups were collected and fixed in an FAS eyeball fixator (Wuhan Servicebio Technology Co., Ltd). The specimens were embedded in paraffin after dehydration, cross-sectioned and stained with hematoxylin and eosin according to the standard protocol. The morphologies of the cornea were observed using a microscope (EVOS FLc). The thicknesses of epithelium and stroma were measured using Nano Measure software.

### 3.14. Anti-inflammation effects of mExo@AA

In this study, the anti-inflammation of mExo@AA was improved *in vitro* and *in vivo*. The anti-inflammation effect *in vitro* was assessed by comparing the M2 rates after treatment. Mouse peritoneal macrophages were isolated as described previously and seeded in 6-well plates.<sup>40</sup> After culturing for 24 h, the medium was changed to DMEM containing lipopolysaccharide (LPS, 1 µg mL<sup>-1</sup>) and co-incubated for 6 h to induce inflammation. After that, the culture media were removed. The cells were washed twice with PBS and re-incubated with fresh media containing saline, mExo (1 mg mL<sup>-1</sup>), AA (509 nM mL<sup>-1</sup>) and mExo@AA (1 mg mL<sup>-1</sup>) for 24 h. The cells were harvested and washed with PBS containing 1% FBS and 1% HEPES and stained with F4/80-Cy5.5 and CD206-FITC antibodies for 30 min at room temperature. Flow cytometry (Becton-Dickinson FACSCalibur) was used to analyze macrophage polarization states.

In order to observe the anti-inflammation in mouse eyes, the mice were euthanized after 7 days of the therapy. The cornea was frozen with liquid nitrogen for 1 min and stored at -20 °C. After the cryosections, the samples were blocked with 0.5% Triton X-100/5% bovine serum albumin for 2 h at room temperature. The samples were incubated with primary antibodies (anti-CD206, Abcam) overnight at 4 °C and then with secondary antibodies (anti-rabbit IgG Alexa Fluor 555) for 1 h. Fluorescence microscopy images were obtained using a confocal microscope (Leica, Germany).

### 3.15. Measurement of tear fluid samples on the human or murine ocular surface

Tear samples were collected by flushing the ocular surface with saline solution and then using a microcapillary tube. More specifically, a 60 µL drop of saline for humans or a 10 µL drop of silane for mice was added to the ocular surface for 10 s, followed by capillary collection. Compared with direct collection using a microcapillary tube, this method is convenient and fast, does not irritate the eye surface, and avoids the production of excessive, ineffective tears. The tear fluid samples obtained from healthy eyes were used as a control. The tear fluid samples were rapidly frozen at -80 °C until assayed. The concentrations of cytokines interleukin-6 (IL-6) and IL-1β in the samples were measured using an ELISA kit (Beijing Solarbio Science & Technology).

### 3.16. Measurement of cellular reactive oxygen on the human ocular surface

The 2',7'-dichlorodihydrofluorescein diacetate (DCFH-DA; Beijing Solarbio Science & Technology) assay kit was used to measure cellular ROS production according to the manufacturer's protocol. In detail, a semicircular piece of cellulose acetate filter paper ( $d = 5$  mm; Whatman) was applied to the lower nasal bulbar conjunctiva adjacent to the corneal limbus under topical anesthesia with 0.5% proparacaine hydrochloride. After 10 s, the paper was quickly placed into a tube containing 190 µL of DMEM. The cells were incubated in the dark with 10 µmol L<sup>-1</sup> of DCFH-DA for 20 min at 37 °C. The DCF fluorescence intensity was then measured at an excitation wavelength of 488 nm and an emission wavelength of 525 nm.

### 3.17. Statistical analysis

The data were presented as the means ± SEM. The data were collected with GraphPad Prism 5.0 software (La Jolla, CA, USA) and analyzed by using one-way analysis of variance (ANOVA) to determine the *p* value (\*\*\**p* < 0.0001, \*\**p* < 0.001, \**p* < 0.01, \**p* < 0.05).

### 3.18. Study approval

The collection and measurement of tear and cell samples were approved by the Ethics Committee of Beijing Chaoyang Hospital (approval ID: 2021-S-626-1). The mouse experiments were reviewed and approved by the Animal Ethics Committee of the Institute of Process Engineering (approval ID: IPEAECA2021103). This study was performed in strict accordance with the Regulations for the Care and Use of Laboratory Animals and Guideline for Ethical Review of Animal (China, GB/T 35892-2018).

## 4. Conclusions

In this study, we developed a new eyedrop (mExo@AA) that combines the dominant corneal repair and anti-inflammation functions of mExo, and the ROS scavenging ability of AA, and investigated its efficacy as a potential therapeutic agent for DED. Characterization of the mExo@AA product showed that AA was successfully loaded onto the mExo with a maximum loading efficacy of about 509 nM mg<sup>-1</sup>. Further experiments indicated that mExo@AA showed good biosafety even at a high concentration of 1 mg mL<sup>-1</sup>. Additionally, the *in vitro* and *in vivo* experiments indicated that mExo@AA had a superior capacity to promote corneal cell growth, scavenge ROS, and inhibit inflammation compared to either of its components alone. Thus, we provide convincing evidence that mExo@AA can potentially be used as an effective therapeutic agent for DED. Notably, mExo@AA not only ameliorated DED symptoms, but also reversed DED-associated pathological changes at both the cellular and tissue levels. In conclusion, mExo@AA is presented as a potential new class of drugs for the treatment of DED, but due to the complexity of DED, the detailed mechanism of action of mExo@AA on DED remains to be explored.





## Author contributions

Y. Tao: supervision of the entire project. F. Ma and J. Feng: methodology and writing – original draft. X. Liu and Y. Tian: investigation. F. X. Luan, Y. J. Wang and W. Q. Yang: data curation. J. Y. Bai and Y. Q. Zhang: writing – review and editing.

## Conflicts of interest

There are no conflicts to declare.

## Acknowledgements

The authors thank Prof. Wei Wei (State Key Laboratory of Biochemical Engineering, Institute of Process Engineering, Chinese Academy of Sciences) for the experimental and technical suggestions.

This work was supported by the National Natural Science Foundation of China (82070948, 82101138, and 82101142), China Postdoctoral Science Foundation (2021M692250), Beijing Hospitals Authority's Ascent Plan (DFL20220301), Shunyi District "Beijing Science and Technology Achievements Transformation Coordination and Service Platform" Construction Fund (SYGX202010), Beijing Hospitals Authority Youth Programme (QML20190303), Basic and Applied Basic Research Foundation Guangdong Province (2019A1515110291).

## References

- J. A. Smith, *Ocul. Surf.*, 2007, **5**, 93–107.
- F. Stapleton, M. Alves, V. Y. Bunya, I. Jalbert, K. Lekhanont, F. Malet, K. S. Na, D. Schaumberg, M. Uchino, J. Vehof, E. Viso, S. Vitale and L. Jones, *Ocul. Surf.*, 2017, **15**, 334–365.
- P. Song, W. Xia, M. Wang, X. Chang, J. Wang, S. Jin, J. Wang, W. Wei and I. Rudan, *J. Glob. Health*, 2018, **8**, 020503.
- V. Valim, V. F. Trevisani, J. M. de Sousa, V. S. Vilela and R. Belfort Jr., *Clin. Rev. Allergy Immunol.*, 2015, **49**, 288–297.
- L. Huang, H. Gao, Z. Wang, Y. Zhong, L. Hao and Z. Du, *Int. J. Nanomed.*, 2021, **16**, 3613–3631.
- N. Song, M. Scholtemeijer and K. Shah, *Trends Pharmacol. Sci.*, 2020, **41**, 653–664.
- B. Mead and S. Tomarev, *Stem Cells Transl. Med.*, 2017, **6**, 1273–1285.
- Q. Wei, Y. Wang, K. Ma, Q. Li, B. Li, W. Hu, X. Fu and C. Zhang, *Stem Cell Rev. Rep.*, 2022, 1025–1040.
- B. F. Hettich, M. Ben-Yehuda Greenwald, S. Werner and J. C. Leroux, *Adv. Sci.*, 2020, **7**, 2002596.
- B. Zhang, M. Wang, A. Gong, X. Zhang, X. Wu, Y. Zhu, H. Shi, L. Wu, W. Zhu, H. Qian and W. Xu, *Stem Cells*, 2015, **33**, 2158–2168.
- T. Zhou, C. He, P. Lai, Z. Q. Yang, Y. Liu, H. Y. Xu, X. J. Lin, B. Y. Ni, R. Ju, W. Yi, L. Y. Liang, D. Q. Pei, C. E. Ekwuagu and X. L. Liu, *Sci. Adv.*, 2022, **8**, eabj9617.
- J. Zhao, X. Li, J. Hu, F. Chen, S. Qiao, X. Sun, L. Gao, J. Xie and B. Xu, *Cardiovasc. Res.*, 2019, **115**, 1205–1216.
- K. Y. Han, J. A. Tran, J. H. Chang, D. T. Azar and J. D. Zieske, *Sci. Rep.*, 2017, **7**, 40548.
- L. Bai, H. Shao, H. Wang, Z. Zhang, C. Su, L. Dong, B. Yu, X. Chen, X. Li and X. Zhang, *Sci. Rep.*, 2017, **7**, 4323.
- G. Wang, H. Li, H. Long, X. Gong, S. Hu and C. Gong, *Ophthalmic Res.*, 2022, **65**, 40–51.
- S. Seen and L. Tong, *Acta Ophthalmol.*, 2018, **96**, e412–e420.
- R. Perez-Garmendia, A. Lopez de Eguileta Rodriguez, I. Ramos-Martinez, N. M. Zuniga, R. Gonzalez-Salinas, H. Quiroz-Mercado, E. Zenteno, E. R. Hernandez and L. F. Hernandez-Zimbron, *Oxid. Med. Cell. Longevity*, 2020, **2020**, 6286105.
- F. Yu, M. Zheng, A. Y. Zhang and Z. Han, *J. Controlled Release*, 2019, **315**, 40–54.
- Q. Zheng, L. Li, M. Liu, B. Huang, N. Zhang, R. Mehmood, K. Nan, Q. Li, W. Chen and S. Lin, *Chem. Eng. J.*, 2020, **398**, 125621.
- R. F. Brubaker, W. M. Bourne, L. A. Bachman and J. W. McLaren, *Invest. Ophthalmol. Visual Sci.*, 2000, **41**, 1681–1683.
- H. S. Min, J. W. Kwon, W. R. Wee, Y. K. Han and H. L. Jin, *Cornea*, 2008, **27**, 916–922.
- P. Gunby, *JAMA, J. Am. Med. Assoc.*, 1980, **243**, 623.
- M. Y. Lee and S. K. Chung, *Cornea*, 2012, **31**, 1165–1169.
- Y. W. Cho, W. S. Yoo, S. J. Kim, I. Y. Chung, S. W. Seo and J. M. Yoo, *Medicine*, 2014, **93**, e125.
- J. Chen, J. Lan, D. Liu, J. Ludvig, L. J. Backman, W. Zhang, Q. Zhou and P. Danielson, *Stem Cells Transl. Med.*, 2017, **6**, 1356–1365.
- X. Ji, X. Song, J. Li, Y. Bai, W. Yang and X. Peng, *J. Am. Chem. Soc.*, 2007, **129**, 13939–13948.
- A. Shabbir, A. Cox, L. Rodriguez-Menocal, M. Salgado and E. V. Badiavas, *Stem Cells Dev.*, 2015, **24**, 1635–1647.
- G. Singh, B. P. Mohanty and G. S. Saini, *Spectrochim. Acta, Part A*, 2016, **155**, 61–74.
- K. M. Choi, Y. K. Seo, H. H. Yoon, K. Y. Song, S. Y. Kwon, H. S. Lee and J. K. Park, *J. Biosci. Bioeng.*, 2008, **105**, 586–594.
- S. Zhang, S. J. Chuah, R. C. Lai, J. Hui, S. K. Lim and W. S. Toh, *Biomaterials*, 2017, **156**, 16–27.
- R. F. Brubaker, W. M. Bourne, L. A. Bachman and J. W. McLaren, *Spectrochim. Acta, Part A*, 2000, **41**, 1681–1683.
- D. Zhou, Y. T. Chen, F. Chen, M. Gallup, T. Vijmasi, A. F. Bahrami, L. B. Noble, N. V. Rooijen and N. A. Mcnamara, *Am. J. Pathol.*, 2012, **181**, 753–760.
- M. Eslani, I. Putra, X. Shen, J. Hamouie, A. Tadepalli, K. N. Anwar, J. A. Kink, S. Ghassemi, G. Agnihotri, S. Reshetylo, A. Mashaghi, R. Dana, P. Hematti and A. R. Djalilian, *Stem Cells*, 2018, **36**, 775–784.
- R. N. Williams and C. A. Paterson, *Exp. Eye Res.*, 1986, **42**, 211–218.



- 35 J. Chen, J. Lan, D. Liu, L. J. Backman, W. Zhang, Q. Zhou and P. Danielson, *Stem Cells Transl. Med.*, 2017, **6**, 1356–1365.
- 36 T. Kojima, T. H. Wakamatsu, M. Dogru, Y. Ogawa, A. Igarashi, O. Ibrahim, T. Inaba, T. Shimizu, S. Noda and H. Obata, *Am. J. Pathol.*, 2012, **180**, 1879–1896.
- 37 Z. Lin, X. Liu, Z. Tong, Y. Wang and Z. Liu, *Mol. Vision*, 2011, **17**, 257–264.
- 38 Y. Tian, F. Zhang, Y. Qiu, S. Wang, F. Li, J. Zhao, C. Pan, Y. Tao, D. Yu and W. Wei, *Nat. Biomed. Eng.*, 2021, **5**, 968–982.
- 39 S. Li, Z. Lu, Y. Huang, Y. Wang, Q. Jin, X. Shentu, J. Ye, J. Ji, K. Yao and H. Han, *Adv. Sci.*, 2022, e2200435.
- 40 A. Ray and B. N. Dittel, *J. Visualized Exp.*, 2010, **35**, e1488.

